

# Degradable thiol-acrylate photopolymers: polymerization and degradation behavior of an in situ forming biomaterial

Amber E. Rydholm<sup>a</sup>, Christopher N. Bowman<sup>a,b</sup>, Kristi S. Anseth<sup>a,c,\*</sup>

<sup>a</sup>Department of Chemical and Biological Engineering, Engineering Center, University of Colorado, Room ECCH 111, Campus Box 424, Boulder, CO 80309-0424, USA

<sup>b</sup>Department of Restorative Dentistry, University of Colorado Health Sciences Center, Denver, CO 80045-0508, USA

<sup>c</sup>Howard Hughes Medical Institute, University of Colorado, Boulder, CO 80309-0424, USA

Received 21 August 2004; accepted 24 November 2004

Available online 13 January 2005

## Abstract

Degradable thiol-acrylate photopolymers are a new class of biomaterials capable of rapidly polymerizing under physiological conditions upon exposure to UV light, with or without added photoinitiators, and to depths exceeding 10 cm. These materials are formed in situ, and the versatility of their chemistry affords a high degree of control over the final material properties. For example, variations in monomer mole fractions directly affect the final network molecular structure, varying the time required to achieve complete mass loss from 25 to 100 days, the molecular weight distributions of the degradation products, and the swelling ratios and compressive moduli throughout degradation. Additionally, varying the mole fraction of multifunctional thiol monomer in the initial reaction mixture controls the concentration of reactive sites in the network available for post-polymerization modification of the polymer.

© 2004 Elsevier Ltd. All rights reserved.

**Keywords:** Thiol-acrylate polymerization; In situ cross-linking; Photopolymerization; Hydrolytic degradation; Poly(ethylene glycol)

## 1. Introduction

There is an emerging interest in the development of in situ forming biomaterials for tissue engineering and drug delivery applications. Various mechanisms for forming these materials have been investigated, including ionic crosslinking of alginate [1], thermally induced physical crosslinking of pluronics [2] and poly(*N*-isopropylacrylamide-*co*-acrylic acid) [3], and enzymatic or pH-induced gelation of chitosan [4]. These and a variety of other formation mechanisms all share the common goal of creating biocompatible, chemically

versatile materials capable of maintaining sustained, localized drug delivery or acting as a scaffold for cell encapsulation or seeding [5]. Unfortunately, most of these methodologies and materials also have limited control of the gelation kinetics and material properties. In contrast, covalently crosslinked materials dramatically improve control of the crosslinking density, which subsequently impacts polymer diffusivity and permeability, degradation rate, equilibrium water content, elasticity, and modulus [6], providing materials that can be tailored to more closely mimic the mechanical properties of native tissues.

Extensive research into covalently crosslinked, degradable biomaterial networks has occurred in the past 25 years. Three main polymerization mechanisms are used to form covalently crosslinked polymeric biomaterials, including chain-growth, step-growth, and mixed-mode chain and step growth mechanisms. During

\*Corresponding author. Department of Chemical and Biological Engineering, Engineering Center, University of Colorado, Room ECCH 111, Campus Box 424, Boulder, CO 80309-0424, USA. Tel.: +1 303 492 3147; fax: +1 303 735 0095.

E-mail address: [kristi.anseth@colorado.edu](mailto:kristi.anseth@colorado.edu) (K.S. Anseth).

formation of a typical chain-growth network, active centers rapidly propagate through monomers containing multiple carbon–carbon double bonds to form high-

molecular-weight kinetic chains that are covalently crosslinked (Fig. 1a). The initiating species in these chain-growth systems, typically radicals, are generated

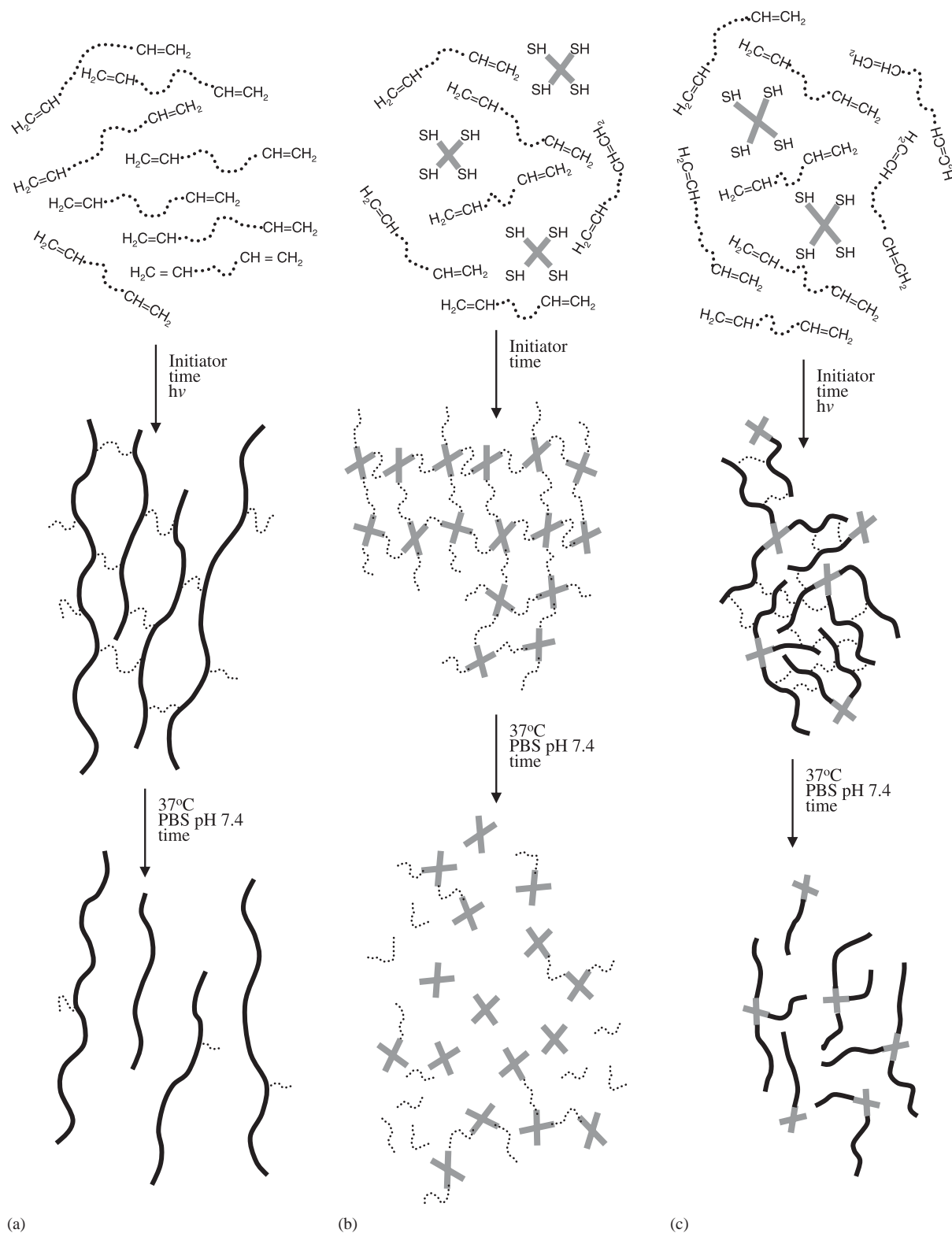


Fig. 1. Pictorial representation of the initial monomer molecules, crosslinked polymer networks, and degradation products for materials formed from (a) chain-growth polymerization mechanism, (b) step-growth polymerization mechanism, and (c) mixed-mode chain and step growth mechanism.

by a variety of methods including thermal energy [7], redox reactions [8], and cleavage of a photoinitiator molecule when irradiated with UV or visible light [5,9]. Photopolymerizations have the added benefit of spatial and temporal control of the polymerization simply through controlling when and where the sample is exposed to the initiating light source. Degradation is incorporated into covalently crosslinked networks through inclusion of hydrolytically cleavable anhydride or ester groups [10–13], or enzymatically cleavable peptide linkages [14–17] in the crosslink segments. For each type of degradable network, the degradation products are comprised of the original monomer core from the starting materials, individual repeat units from the degradable segments, and the high-molecular-weight kinetic chains generated during polymerization (Fig. 1a).

Modifications to the monomer core-chemistry in chain-growth networks directly impact the network's crosslinks and allows degradation behavior, modulus, elasticity, and equilibrium swelling ratios to be tailored [18–20]. For example, highly crosslinked networks formed from low-molecular-weight, hydrophobic dimethacrylated polyanhydrides degrade through a surface erosion mechanism while moderately crosslinked hydrogels formed from high-molecular-weight, hydrophilic dimethacrylated poly(lactic acid)-*b*-poly(ethylene glycol)-*b*-poly(lactic acid) (PEG-PLA) undergo bulk erosion [21–23]. Another example is the ability to tailor the mechanical strength and modulus of oligo(poly(ethylene glycol) fumarate) hydrogels through modifications of the PEG molecular weight [24], crosslinker mole fraction [25], and porogen content [26].

Despite the demonstrated advantages of these polymeric networks, the broader utility of degradable chain-growth biomaterials is limited by several factors. First, only the crosslink segments degrade, leaving high-molecular-weight kinetic chains that must be excreted from the body [22,27]. Second, the molecules used to

generate the active radical centers and initiate polymerization can be cytotoxic, and in certain applications, such as cell, protein, and DNA encapsulation, residual initiator molecules are problematic [28,29]. Additionally, control over the network degradation profile and release behavior is limited due to the network evolution mechanism during chain-growth polymerizations. Finally, for photoinitiated polymers light attenuation by the initiator restricts the maximum attainable cure depth to a few millimeters.

As an alternative to in situ forming networks synthesized via chain-growth polymerizations, Hubbell and coworkers developed degradable networks formed through Michael-addition-type reactions between thiol and acrylate, acrylamide, or vinyl sulfone groups [30–36]. These networks form through a step-growth polymerization of the thiol and vinyl groups (Fig. 1b). The step-growth nature of these Michael-addition reactions stems from a two-part propagation process where a thiolate ion reacts with a vinyl group to form a carbon-based anion, which then reacts with another thiol group to regenerate another thiolate ion. The repetition of these events in a system of multifunctional monomers generates a covalently crosslinked network with better control of the crosslinking density and corresponding material properties than the photoinitiated chain polymerization of acrylates [32]. Additionally, the degradable segments are incorporated throughout the network, eliminating the high-molecular-weight degradation products containing the backbone kinetic chains formed during chain-growth polymerization. The Michael-addition reaction is catalyzed in a slightly basic environment, eliminating the need to add any initiators. Unfortunately, it is not possible to spatially and temporally control network formation in these materials, and the network gelation rates are considerably slower than those exhibited by the photoinitiated chain polymerization of multifunctional macromers (Fig. 2).

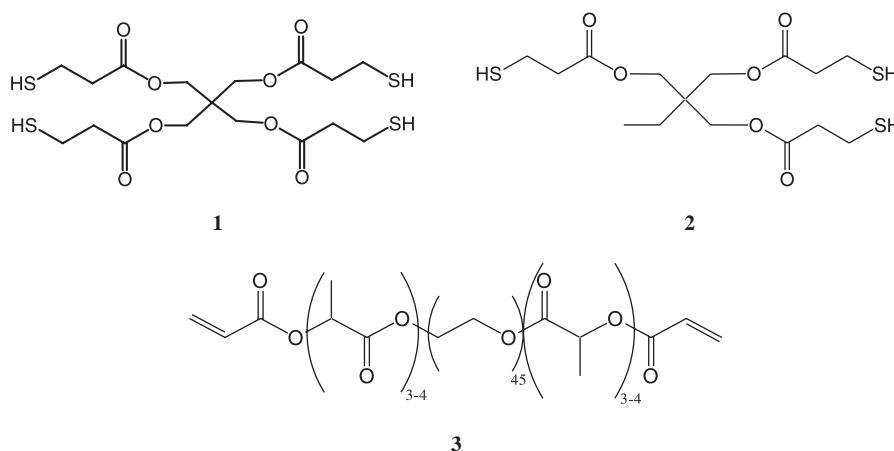
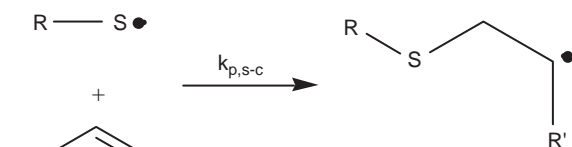


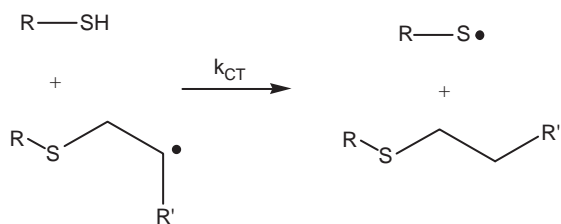
Fig. 2. Multifunctional thiol and degradable PEG-PLA-diacrylate monomers used in this study.

This publication describes a class of degradable thiol-acrylate biomaterials formed through a mixed-mode polymerization mechanism that is a combination of chain-growth and step-growth reactions (Fig. 1c), where both reactions are radically mediated. Three reactions are involved in the propagation mechanism of thiol-acrylate polymerizations and are shown below (Steps 1–3) [37]. Steps 1 and 2 are identical to the classical photoinitiated step growth thiol-ene polymerization in which propagation and chain transfer occur sequentially [38–40]. An additional propagation step occurs in thiol-acrylate polymerizations due to the ability of the acrylate groups to react with carbon-based radicals (Step 3). This additional reaction results in acrylate homopolymerization, similar to the chain-growth polymerization mechanism of pure acrylates. The unique thiol-acrylate molecular structure evolves from the mixed-mode polymerization mechanism and is directly impacted by thiol:acrylate ratios, transitioning from being more chain-like to more step-like as the ratio of thiol to acrylate groups increases.

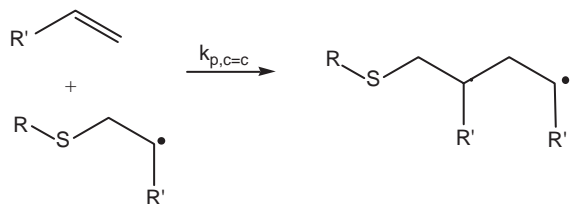
Step 1:



Step 2:



Step 3:



In addition to their unusual mixed-mode polymerization mechanism, thiol-acrylates have a number of unique and attractive attributes. They polymerize upon exposure to UV light, with or without added photoinitiator molecules, allowing samples with thicknesses well in excess of 10 cm to be formed. The use of light to initiate the reaction affords spatial and temporal control of the polymerization. The final mass loss profile and degradation induced swelling behavior are controlled through simple changes to the network structure caused

by variations in thiol:acrylate ratios. Additionally, changing the thiol mole fraction in the network provides control of the final degradation product's molecular weight distribution. Results herein will demonstrate the advantages of degradable thiol-acrylate networks and compare their behavior to degradable networks formed by the chain polymerization of pure acrylate monomer systems.

## 2. Materials and methods

### 2.1. Reagents

Pentaerythritol tetrakis(3-mercaptopropionate) (tetrathiol, Fig. 2 1), trimethylpropane tris(3-mercaptopropionate) (trithiol, Fig. 2 2), and poly(ethylene glycol)  $\bar{M}_n$  2000 (PEG<sub>2000</sub>) were purchased from Aldrich. DL-lactide was purchased from Polysciences, acryloyl chloride from Fluka, stannous 2-ethylhexanoate from Sigma, and monobasic potassium phosphate from Mallinckrodt. Triethylamine, dibasic potassium phosphate, methylene chloride, diethyl ether, and benzene were purchased from Fisher Scientific. The photoinitiator, 1-[4-(2-hydroxyethoxy)-phenyl]-2-hydroxy-2-methyl-1-propane-1-one, or Irgacure 2959 (I2959) was a gift from Ciba. All reagents were used as received with the exception of methylene chloride, which was dried with sodium sulfate (Fisher), vacuum filtered, and stored over molecular sieves (Mallinckrodt).

### 2.2. Poly(ethylene glycol)-*b*-poly(lactic acid)-diacrylate

The diacrylated PEG-PLA macromer studied here (Fig. 2 3) were prepared using techniques similar to those first described by Sawhney et al. [12] and others [6,22,41]. Analysis by <sup>1</sup>H NMR (CDCl<sub>3</sub>): 1.55 ppm (33.86 H, PLA-O-CO-CH-CH<sub>3</sub>-), 3.65 ppm (176.44 H, PEG-O-CH<sub>2</sub>-CH<sub>2</sub>-), 4.27 ppm (4.00 H, last H's on PEG next to PLA block), 5.17 ppm (10.42 H, PLA-O-CO-CH-CH<sub>3</sub>-), 5.9 ppm (dd, 1.59 H, -COO-CH=CH<sub>2</sub>), 6.17 ppm (q, 1.55 H, -COO-CH=CH<sub>2</sub>), 6.47 ppm (dd, 1.61 H, -COO-CH=CH<sub>2</sub>).

### 2.3. Mid-IR polymerization characterization

To observe real-time polymerization kinetics of thin-film samples, FTIR studies were completed using a Nicolet 760 Magna FTIR spectrometer with a KBr beam splitter and MCT/B detector. Samples were prepared by placing thiol and acrylate monomers (0, 15, 30, and 50 mol% thiol functional groups) and 0.1 wt% I2959 into a glass vial, melting the PEG-PLA-diacrylate in a 50 °C water bath while magnetically stirring the molten solution, and sandwiching a drop of the resulting mixture between two NaCl crystals. These

samples were placed in a horizontal transmission apparatus [42] that allowed in situ observations of polymerization behavior during irradiation using series scans that obtained spectra at a rate of 0.67 scans per second. Samples were irradiated with  $5 \text{ mW/cm}^2$  of 320–500 nm light (peak light intensity at 365 nm) using an Ultracure light source (EXFO). To avoid solidification of the monomer mixtures (the PEG-PLA-diacrylate monomer has a melting point of  $35 \pm 2^\circ\text{C}$ ), a custom made temperature apparatus [43] was used to maintain the sample temperature at  $40^\circ\text{C}$ . The acrylate conversion was monitored using both the carbon–carbon double bond absorption double peak at  $1636$  and  $1620 \text{ cm}^{-1}$  and the out of plane stretch at  $810 \text{ cm}^{-1}$ . The thiol conversion was observed by measuring the area of the S–H absorption peak at  $2560 \text{ cm}^{-1}$ . Conversions were calculated using the ratio of the peak area as a function of time to the peak area prior to irradiation. From this technique, acrylate conversion profiles were determined for specimens in duplicate. To determine the  $k_{p,c=c}/k_{CT}$  ratio for these degradable thiol-acrylate materials, seven specimens were averaged for the 2:1 thiol:acrylate data, three specimens for the 3:1 data, and two specimens for the 4:1 data.

#### 2.4. Depth of cure characterization

Rectangular test tubes ( $2 \times 6 \times 110 \text{ mm}^2$ ) were filled with a 85 mol% PEG-PLA-diacrylate and 15 mol% tetrathiol mixture. Using the same FTIR instrument that was used for the mid-IR experiments, near-IR spectra of three specimens were collected using an InGaAs detector and white light IR source. The acrylate conversion was calculated from peak-area changes for the  $6165 \text{ cm}^{-1}$  peak, while the thiol conversion could not be accurately determined for these systems with near-IR. Initial near-IR spectra were obtained at predetermined depths from the top of the test tube prior to irradiation. The test tube was held vertically in a  $40^\circ\text{C}$  water bath, and the end of a light guide from an Acticure light source (EXFO) was positioned directly over the top of the test tube, shining down into its interior. The top of the sample was exposed to  $2.17 \text{ W/cm}^2$  of 365 nm light for varying amounts of time, after which the same depths imaged initially were rescanned using near-IR. This process of equilibrating the sample temperature to  $40^\circ\text{C}$ , exposing to UV light, and obtaining the near-IR spectra was repeated until the sample had been irradiated for a total of 2 h.

#### 2.5. Degrading thiol-acrylate networks

Disks were made by filling molds 5 mm in diameter and 1.7 mm thick with various monomer solutions always containing 0.1 wt% I2959 and 20 wt% DMSO as a solvent in which thiol and ene monomers were

readily soluble and exposing them to  $3.5 \text{ mW/cm}^2$  of 365 nm light for an hour. The initial sample masses were measured, and the disks were placed into labeled tissue cassettes for tracking purposes. The cassettes were placed into large jars according to disk type, covered with pH 7.4 phosphate buffer solution, and the jars were placed in an incubated orbital shaker ( $37^\circ\text{C}$ , 60 rpm). The buffer solution was changed every 1–2 weeks to maintain sink conditions. At specified time points, disks were removed in triplicate; their wet mass measured; their compressive modulus determined using a dynamic mechanical analyzer (DMA 7e with TAC 7/Dx, data analyzed with Pyris software, Perkin-Elmer); and lyophilized (Freezone 4.5, Labconco) to obtain their dry mass. From this data, the mass swelling ratio,  $q$ , was calculated as the ratio of the final wet mass to the final dry mass, and the mass loss was calculated as described previously by Metters et al. [19].

#### 2.6. Calculating the molecular weight of the degradation products

Four or more disks of each thiol-acrylate monomer ratio were degraded in 1.5 mL of 0.5 M NaOH for 3 h. Solutions were neutralized with 8–12 drops of 1 M HCl and transferred to cellulose ester dialysis tubing (Spectra/Por, Spectrum Laboratories) with a 500 Da molecular weight cut off, to remove any NaCl while retaining low-molecular-weight degradation products. The dialysis tubes were placed in a large excess of deionized water (2–10 L) for a minimum of 48 h, during which the bulk solution was changed twice. Samples were removed from the tubing, frozen, and lyophilized, producing a small amount of white powder from which the PEG chains were removed via chloroform extraction. The final degradation products were filtered from the chloroform, dissolved in 0.1 M  $\text{NaNO}_3$  buffer, and characterized using gel permeation chromatography (GPC: system: Waters 515 HPLC pump, 2410 refractive index detector. Columns: Suprema 30A, 100A, 1000A, and Linear XL from Polymer Standards Service, USA) calibrated with poly(methacrylic acid) (PMAA) molecular weight standards (Polymethacrylic Acid Sodium Salt,  $M_p = 1000$ – $1,000,000$ , Polymer Standards Service, USA, where  $M_p$  is the molecular weight at the peak maximum).

#### 2.7. Statistical analysis

A two-sided Student's  $t$ -test with equal variance was used to determine confidence intervals for the statistical analysis shown (Microsoft Excel). Fisher's least significant difference comparison of means was used to compare means in Table 3.

### 3. Results and discussion

#### 3.1. Thiol-acrylate polymerization behavior

Thiol-acrylate photopolymerizations occur very rapidly, even when initiated with relatively low initiator concentrations and light intensities, enabling the formation of networks under physiologically relevant conditions and time scales. The conversion profile of the acrylate homopolymerization (Fig. 3d) displays classical features of multifunctional-monomer chain polymerizations: rapidly reacting upon exposure to UV light, exhibiting autoacceleration and autodeceleration as polymerization continues, and reaching a maximum conversion of 95% in approximately 90 s. Interestingly, when thiol is added to the initial monomer mixture, the polymerization is even more rapid, reducing the time required to reach 95% conversion to 60 s. Moreover, the delay in acrylate homopolymerization, typically attributed to oxygen inhibition of the radical polymerization, is minimized or completely eliminated by the addition of the thiol monomer.

Additionally, thiol-acrylate polymerization times are significantly faster than those reported previously for biomaterials formed via Michael-addition due to the high reactivity of the initiating radical species used in the photopolymerizations [32,36]. The 60 s required for thiol-acrylate samples to reach 90% conversion (Fig. 3) is much faster than the 1–2 h required for optimal crosslinking efficiency of the Michael-addition materials [32]. Decreasing cure times so significantly is a distinct advantage for in situ forming biomaterials, directly impacting implantation-procedure duration. Also, unlike the Michael-addition reactions that begin as soon as

base is added to the monomer mixture, photopolymerization of degradable thiol-acrylate is easily controlled spatially and temporally by controlling when and where the initiating UV-light irradiates the sample. As a result, multilayered, three-dimensional devices with complex patterns and geometries can be fabricated from these degradable thiol-acrylate materials, and for applications where temporal control is critical, polymerization will not occur until the monomer mixture is exposed to UV light.

Thiol conversion and the relative consumption rates of thiol and acrylate groups were determined to confirm that the mixed mode mechanism is responsible for thiol-acrylate photopolymerization. Normally, thiol and acrylate conversion data are each distinctly determined by independently monitoring the disappearance of their absorbance peaks in the IR spectra. For the data shown in Fig. 3, determining thiol conversions in this way was difficult because the thiol monomers contribute less than 5% of the mass in these networks, resulting in a small, relatively insignificant thiol absorption peak. To overcome this limitation, samples with a large excess of thiol groups were investigated, increasing the size of the thiol peak and allowing its change in area to be quantified. Thiol conversions calculated from these excess-thiol experiments are shown in Fig. 4 as a function of acrylate conversion. Cramer et al. [37] determined the relative consumption rate of thiol and acrylate groups (Eq. (1)) in non-degradable systems and found the ratio of  $k_{p,c} = c/k_{CT}$  to be 1.5. Using this value for  $k_{p,c} = c/k_{CT}$ , the experimentally measured conversion profiles (Fig. 4) were predicted very well for degradable thiol-acrylate networks with excess thiol groups. For network

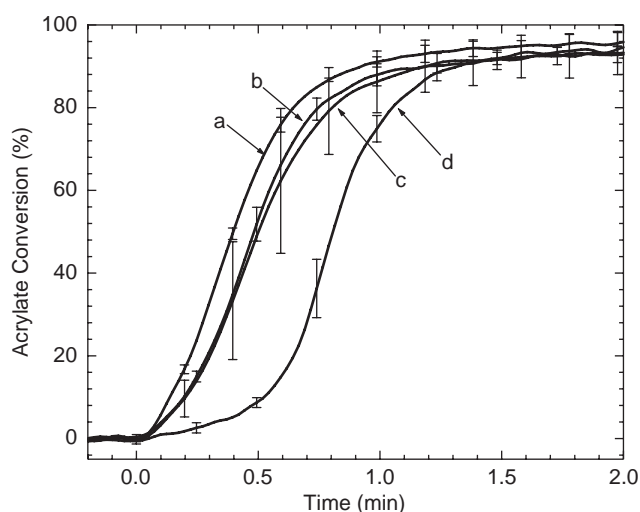


Fig. 3. Acrylate conversion profiles of mixtures containing (a) 50, (b) 30, (c) 15, and (d) 0 mol% tetrathiol. Each sample was prepared with 0.1 wt% I2959 initiator, heated to 40 °C, and irradiated with 5.0 mW/cm<sup>2</sup> 320–500 nm light. Error bars represent standard deviations of two replicates.

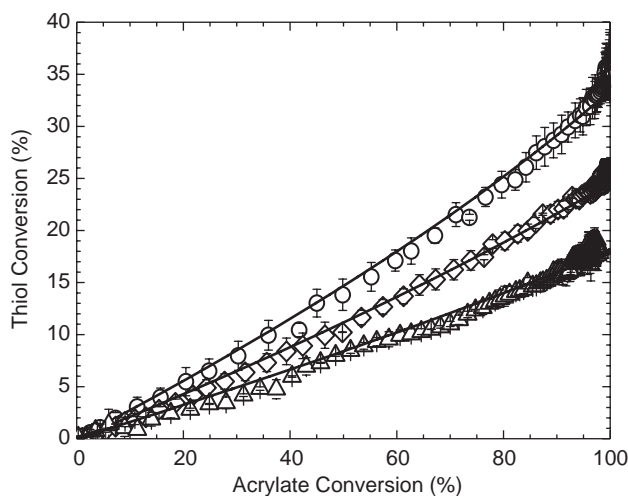


Fig. 4. Comparison of model predictions (—) and experimentally measured thiol-acrylate conversions with thiol: acrylate mole ratios of 2:1 (○), 3:1 (◇), and 4:1 (△) assuming  $k_{p,c} = c/k_{CT} = 1.5$ . Each sample was prepared with 20 wt% DMSO, 0.1 wt% I2959 initiator, and irradiated with 5.0 mW/cm<sup>2</sup> 320–500 nm light. Error bars represent standard deviations of 7, 3, and 2 specimens for the 2:1, 3:1, and 4:1 thiol-acrylate samples, respectively.

Table 1  
Experimental and theoretical final thiol conversions for various initial thiol:acrylate molar ratios

[SH] <sub>0</sub> : [C=C] <sub>0</sub>	Final conversion (%)	
	Acrylate	Thiol
4:1	100 ± 0.31	19 ± 0.31 <sup>a</sup>
3:1	100 ± 0.59	23 ± 0.34 <sup>a</sup>
2:1	100 ± 0.24	38 ± 0.59 <sup>a</sup>
1:1	96 ± 0.33	52 <sup>b</sup>
3:7	93 ± 0.30	67 <sup>b</sup>
15:85	94 ± 0.32	78 <sup>b</sup>

<sup>a</sup>Experimentally determined final thiol and acrylate conversions from FTIR experiments.

<sup>b</sup>Calculated final thiol conversion from experimentally measured final acrylate conversion using Eq. (1).

compositions where the thiol IR absorption peak was too small to measure accurately, final thiol conversions were approximated using Eq. (1), a  $k_{p,c=c}/k_{CT}$  of 1.5, and experimentally measured acrylate conversions (Table 1). In Eq. (1), [C=C] and [SH] are the acrylate and thiol group concentrations and  $k_{p,c=c}$  and  $k_{CT}$  are the propagation and hydrogen abstraction kinetic rate constants:

$$\frac{d[C=C]}{d[SH]} = 1 + \left( \frac{k_{p,c=c}}{k_{CT}} \right) \frac{[C=C]}{[SH]} \quad (1)$$

Despite the large number of unreacted thiol groups predicted by this method for samples in Table 1, the multifunctionality of the thiol monomers leads to very low percentages of extractable thiol monomers. For example, for networks prepared from monomer mixtures containing 50 mol% thiol groups, statistically only 5% of the initial thiol monomer molecules have all four thiol groups unreacted and are extractable from the polymerized network. As the initial thiol concentration decreases to 30 mol%, the number of extractable tetrathiol monomers decreases to 1%.

The unequal consumption of thiol and acrylate groups for mixtures having 1:1 ratios of thiol and acrylate functional groups, the increase in final thiol conversion with decreasing initial thiol mole fraction for all molar ratios shown in Table 1, and an experimentally determined  $k_{p,c=c}/k_{CT}$  of 1.5 all confirm that a mixed mode chain and step growth polymerization mechanism is occurring during degradable thiol-acrylate network formation.

Besides confirming the mixed-mode polymerization mechanism, an examination of the kinetic rate constants in Eq. (1) explains the increase in reaction rates for thiol-containing networks observed in Fig. 3. As shown in Fig. 4, the propagation rate of a carbon-based radical through another carbon-carbon double bond relative to the rate of chain transfer with a thiol group

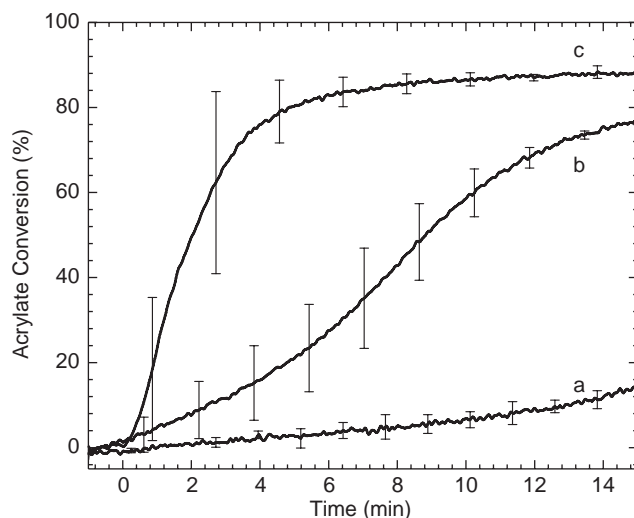


Fig. 5. Conversion profile of initiatorless photopolymerizations: (a) 100% PEG-PLA-diacrylate, light intensity = 5 mW/cm<sup>2</sup> at 320–500 nm, (b) 85 mol% PEG-PLA-diacrylate, 15 mol% tetrathiol, light intensity = 5 mW/cm<sup>2</sup>, (c) 85 mol% PEG-PLA-diacrylate, 15 mol% tetrathiol, light intensity = 50 mW/cm<sup>2</sup>. Error bars represent standard deviations of two replicates.

( $k_{p,c=c}/k_{CT}$ ) is 1.5. The ratio of thiol radical propagation to chain transfer ( $k_{p,s-c}/k_{CT}$ ) for thiol-acrylate networks is 13 [44]. Therefore, the ratio of thiol radical reactivity to carbon radical reactivity ( $k_{p,s-c}/k_{p,c=c}$ ) is approximately 8.7. Since the reaction of a thiol radical with a carbon-carbon double bond is nearly an order of magnitude faster than the reaction of a carbon-based radical with the same double bond, the acrylate polymerization rate increases with the addition of the thiol into the polymerization mixture.

In addition to rapidly polymerizing under standard reaction conditions, thiol-acrylate monomers are directly photopolymerizable without the addition of a separate initiating species (Fig. 5). In contrast to the homopolymerization of the PEG-PLA-diacrylate monomer (curve a), which only shows 15% conversion after exposure to UV light in the absence of photoinitiator, samples containing 15 mol% tetrathiol reach 75% conversion under the same reaction conditions (curve b). Increasing the light intensity by an order of magnitude further increases the final conversion to 90% and dramatically decreases the polymerization time to the extent that it starts to approach that of the initiator-containing systems (curve c). Comparing the time required for each system to reach 75% conversion (Table 2) further indicates that the addition of thiol to initiatorless acrylate monomers dramatically decreases cure time. Rapid photopolymerization in the absence of photoinitiators has also been observed for a variety of non-degradable thiol-acrylate and thiol-ene systems [37,44–48].

Bryant et al. [28] demonstrated the link between the number of radicals generated by photoinitiator molecules and cell viability for several UV photoinitiating systems. One cytocompatible photoinitiating system was identified, which used 0.05 wt% 1-[4-(2-hydroxyethoxy)-phenyl]-2-hydroxy-2-methyl-1-propane-1-one, or Irgacure 2959 (I2959) and 5–10 mW/cm<sup>2</sup> of 365 nm UV light, and is currently used by several research groups to encapsulate cells. However, to minimize potential problems with residual photoinitiator and light attenuation effects during the polymerization of thick samples, initiator-free samples are desirable. Furthermore, investigations of photopolymerized networks for localized, sustained DNA delivery [29] highlight the damaging effects initiators have on plasmid DNA. Previously, these effects have been mitigated with the

inclusion of radical scavengers into the monomer solution or complexation of the DNA to transfection agents. For cell encapsulation, plasmid DNA delivery, and potentially protein delivery, it is possible that using initiatorless thiol-acrylate networks would improve encapsulated cell viability and delivered DNA/protein activity.

An added benefit of initiatorless thiol-acrylate polymerizations is the ability to cure these materials to much greater depths than networks containing photoinitiators due to the absence of photoinitiator light attenuation. As shown in Fig. 6, initiatorless, degradable thiol-acrylate networks are curable to depths exceeding 10 cm (samples up to 25 cm have previously been formed for non-degradable thiol-ene systems [45]), demonstrating the advantages of using initiatorless thiol-acrylate networks when thick gels are desired. In these materials polymerization proceeds more rapidly at the top of the sample, where light intensity is greatest, but decreases at greater depths in the sample. Continued exposure leads to complete polymerization of the sample.

Table 2

Time to reach 75% acrylate conversion in initiatorless thiol-acrylate networks

Sample	Time to reach 75% acrylate conversion (min)
15 mol% thiol, 50 mW/cm <sup>2</sup>	3.6 ± 1.7
15 mol% thiol, 5 mW/cm <sup>2</sup>	14.0 ± 0.4
0 mol% thiol, 5 mW/cm <sup>2</sup>	27.1 ± 2.8

Error is standard deviation,  $n = 2$ ,  $\alpha \geq 0.01$ .

### 3.2. Degradable thiol-acrylate material properties

For most tissue engineering and drug delivery applications, well-characterized biomaterials with controllable degradation behavior are desirable. Metters

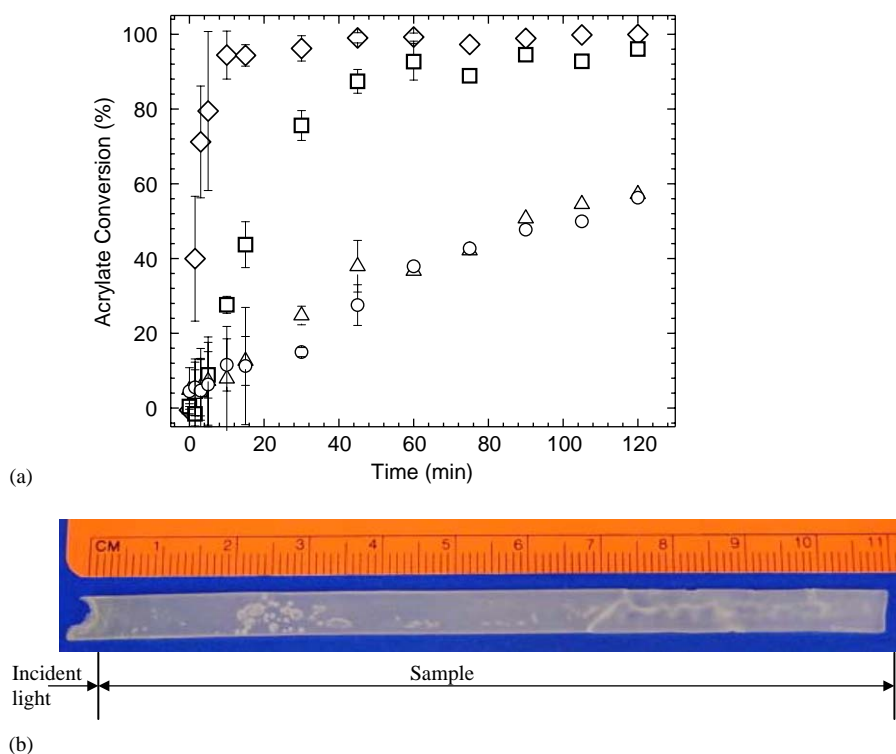


Fig. 6. (a) Conversion profiles at different distances from the initiating light source. Samples are made from a 15 mol% tetrathiol, 85 mol% PEG-PLA-diacrylate monomer mixture that contains no solvent and no initiator. Samples were polymerized with 2.2 W/cm<sup>2</sup> of 320–500 nm light at 40 °C. Top surface =  $\diamond$ , 3 cm from top =  $\square$ , 6 cm from top =  $\Delta$ , 9 cm from top =  $\circ$ . Error bars represent standard deviations of three replicates. (b) Polymerized sample, removed from rectangular test tube.

Table 3  
Effect of thiol concentration in PEG-PLA-diacrylate-trithiol networks on mass loss, equilibrium swelling ratio, and compressive modulus

Thiol mol%	Time to 10% mass loss (days)	Time to 90% mass loss (days)	Time when $q = 10$ (days)	Initial compressive modulus (kPa)
0	10.0 ± 1.9	45.8 ± 0.8 <sup>a</sup>	31.4 ± 0.6 <sup>b</sup>	3410 ± 270
5	11.6 ± 2.2	48.3 ± 0.4 <sup>a</sup>	32.9 ± 0.5 <sup>a</sup>	3850 ± 120 <sup>c</sup>
15	11.7 ± 0.4	42.9 ± 0.7 <sup>a</sup>	30.7 ± 0.2 <sup>b</sup>	3380 ± 440
30	9.4 ± 1.4	31.5 ± 0.1 <sup>a</sup>	24.3 ± 1.0 <sup>a</sup>	2990 ± 280

Samples were disks 5 mm in diameter and 1.7 mm thick. Each polymer composition was prepared in 20 wt% DMSO with 0.1 wt% I2959.

<sup>a</sup>Statistically different than all other sample types for  $\alpha \geq 0.01$ .

<sup>b</sup>0 and 15 mol% thiol are not significantly different from each other for  $\alpha \geq 0.05$ .

<sup>c</sup>Statistically different than all other sample types for  $\alpha \geq 0.05$ .

et al. [19,22,41] demonstrated the impact of monomer and solvent concentrations on network structure and the resulting control of degradation behavior for the chain polymerization of PEG-PLA-diacrylate monomers. In condensation gels formed through thiol-acrylate Michael addition reactions, Elbert et al. [31] observed increasing swelling behavior and hydrolytic degradation rates with decreasing monomer functionality and increasing solvent concentration, and Lutolf et al. [33] examined how variations in sensitivity to cell-secreted proteases in the network crosslinks impact enzymatic degradation rates.

In thiol-acrylate photopolymer networks, changing thiol mole fraction controls network structure and observable material properties such as mass loss, mass swelling ratio, and compressive modulus throughout degradation. The data in Table 3 demonstrate the effect of thiol concentration on mass loss, equilibrium swelling ratio, and compressive modulus. At early stages of degradation, the mass loss data and the initial modulus values for the 0, 15, and 30 mol% thiol samples are indistinguishable at the 95% confidence interval. As degradation continues, increasing thiol concentration decreases both the time required to reach 90% mass loss and complete erosion of the sample, and the time required for the polymer to degrade and swell to 90% water (mass swelling ratio,  $q$ , of 10).

These observed changes in mass loss, equilibrium swelling, and compressive modulus with thiol mole fraction variations are directly related to the mixed-mode polymerization mechanism used to form these materials and the resulting molecular structure of the network. As explained by Metters et al. [22], mass loss behavior is correlated to the rate at which PLA crosslinks hydrolyze and the number of crosslinks that need to degrade before PEG and polyacrylate segments are released from the network. The swelling ratio

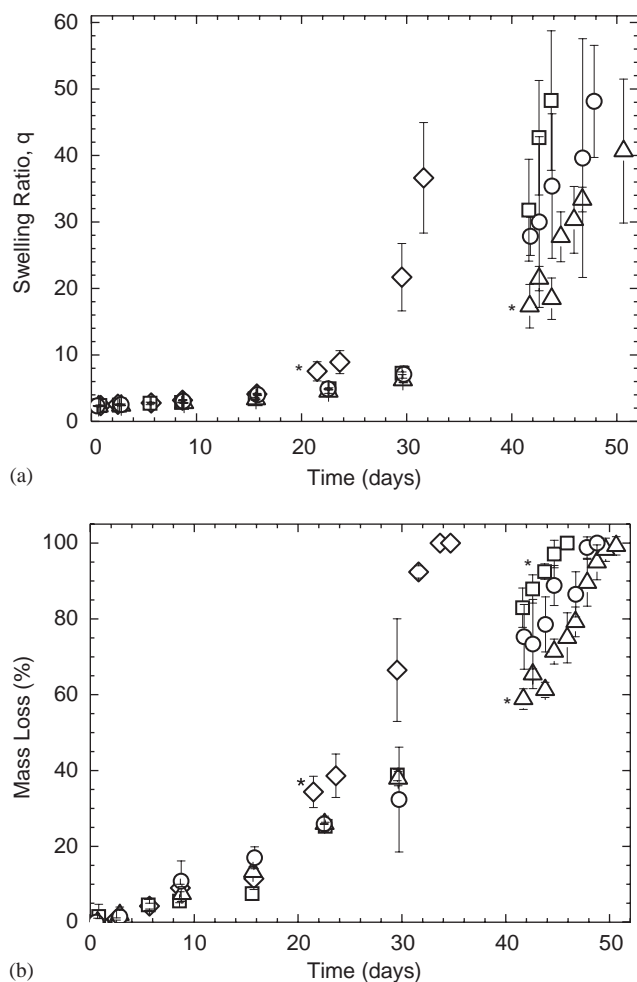


Fig. 7. (a) Equilibrium mass swelling ratio ( $q$ ) and (b) mass loss as a function of time for polymer networks containing 30 mol% trithiol ( $\diamond$ ), 15 mol% trithiol ( $\square$ ), 5 mol% trithiol ( $\Delta$ ), and no thiol ( $+$ ). All samples were prepared from monomer mixtures containing 20 wt% DMSO and 0.1 wt% I2959 and were degraded in pH 7.4 phosphate buffered saline. Error bars represent standard deviations of three replicates. \*Denotes first time point where the sample is statistically different from the other sample types at the 95% confidence interval based on a standard  $t$ -test.

depends on the network's crosslink density, while the compressive modulus is a function of both swelling ratio and crosslinking density. Fig. 7 details the impact of thiol concentration on mass loss and swelling behavior.

Equilibrium swelling is inversely dependent on crosslinking density: as degradation proceeds and the ester bonds within the crosslink's PLA blocks hydrolyze, the crosslinking density decreases, and the network equilibrium swelling ratio increases. Within the first 10 days the equilibrium swelling ratios of the four networks studied in Fig. 7a are not distinguishable, indicating similar initial crosslinking densities and initial solvent concentrations despite variations in thiol-group concentration, as expected.

At early time points this swelling behavior is expected since variations in network structure due to thiol mole fraction do not impact rates of PLA hydrolysis or bulk crosslinking density. As degradation progresses, however, the impact of thiol concentration becomes apparent. Increasing the number of thiol groups increases the amount of chain transfer occurring during polymerization, shortening the thiol-polyacrylate chains and reducing the number of crosslinks attached to each kinetic chain. As degradation progresses to the point where kinetic chains are no longer attached to the network, swelling dramatically increases, and the time where this release occurs increases with decreasing thiol concentration. The exception to this behavior is the 5 mol% thiol samples, which exhibit delayed increases in equilibrium swelling compared to the 0 mol% data. Small additions of thiol to acrylate networks increase the final conversion [37] and the crosslinking density, reversing the expected trends in degradation behavior. At higher thiol concentrations, increases in final conversion due to the thiol are offset by the dramatic reduction in kinetic chain lengths due to increased chain transfer.

Similarly, at early time points, all four thiol-acrylate networks have similar mass loss profiles resulting from a relatively identical crosslinking density and similar PLA-hydrolysis rates. Mass lost during this portion of degradation (0–10 days), is attributed to the lactic acid units released from the network through hydrolysis of

multiple ester bonds within one PLA block, and the crosslink's PEG core released when one or more ester bonds have hydrolyzed in each PLA block connecting it to the thiol-polyacrylate kinetic chains (Fig. 8). As degradation proceeds, the network structure and molecular weight of the kinetic chains start to influence the mass loss profiles. When crosslink cleavage has progressed to the point where a significant number of kinetic chains are no longer attached to the polymer network and their release is also contributing to the mass loss profile, the mass loss rate increases rapidly and the network undergoes reverse gelation. Networks with shorter kinetic chains have fewer crosslinks that must degrade before this collapse occurs (Fig. 8), enabling the mass loss profile and time for complete mass loss to be controlled through alterations in initial thiol-acrylate monomer composition.

As the thiol-acrylate polymers degrade, degradation products are released from the network. From a clinical point of view, control of degradation product molecular weight is desirable for natural elimination of the polymer from the body to occur [27]. Complete degradation of thiol-acrylate networks produces lactic acid units, the PEG core of each crosslink, and high-molecular-weight polyacrylate or thiol-polyacrylate chains form during photopolymerization. While PEG and PLA size are easily manipulated through monomer selection and synthesis conditions, the molecular weight of the kinetic chains depends on the photopolymerization

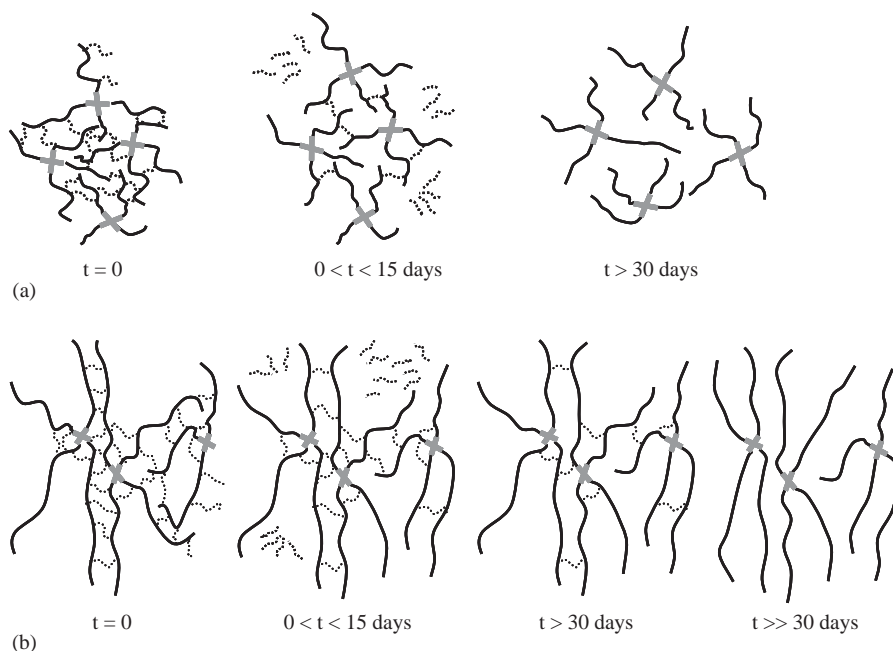


Fig. 8. Hydrolytic degradation of a mixed-mode thiol-acrylate network having (a) a high thiol:acrylate ratio (3:7), and (b) a low thiol:acrylate ratio (1:19). Initially, the two networks have similar crosslinking density and swelling. At early degradation times (less than 15 days) the only mass lost is from the PEG core of the crosslinks, resulting in similar mass loss and swelling behavior. The time when enough crosslinks have degraded for kinetic chains to be released from the network increases with decreasing thiol concentration. For each schematic, the dashed lines represent degradable PEG-PLA-diacrylate crosslinks, the solid black represent polyacrylate chains (kinetic chains), and the gray X's represent tetrathiol monomers.

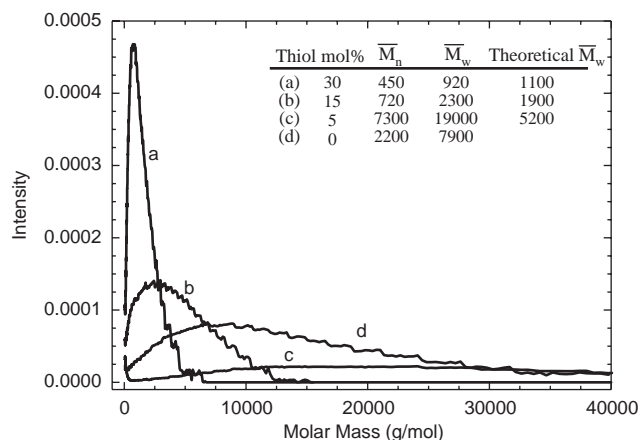


Fig. 9. GPC data for the thiol-polyacrylate kinetic chains from degraded PEG-PLA-diacrylate-trithiol networks. Molar mass values are based on poly(methacrylic acid) standards. Data normalized to identical peak area for each sample: (a) 30 mol% trithiol, (b) 15 mol% trithiol, (c) 5 mol% trithiol, (d) no thiol. One specimen was tested for each sample type.

conditions, including the thiol mole fraction in thiol-acrylate networks.

To explore this phenomenon experimentally, cross-linked PEG-PLA-diacrylate disks made with varying thiol concentrations and functionalities were degraded in 0.5 N sodium hydroxide. The kinetic chains were first isolated using dialysis and chloroform extraction and then analyzed with aqueous gel permeation chromatography (GPC). Theoretical values for the kinetic chain's molecular weights were approximated from the weight average degree of polymerization ( $\bar{X}_w$ , number of acrylates that react with each thiol group, determined numerically using Eq. (1)), and the corresponding thiol and acrylic acid molecular weights. These values are similar to the experimentally measured GPC values for an instrument calibrated with linear poly(methacrylic acid) standards. The GPC results shown in Fig. 9 also indicate that adding thiol reduces the molecular weight and polydispersity of the kinetic chains. These observations are attributed to changes in network structure caused by the mixed mode network formation and the chain-transfer behavior of the thiol groups during polymerization.

#### 4. Conclusions

Photopolymerized, degradable thiol-acrylate networks represent a novel class of biomaterials with distinct advantages over the PEG-PLA-(meth)acrylate and Michael-addition networks previously investigated. They rapidly polymerize when exposed to UV light, and enable spatial and temporal control of the polymerization through masking or shuttering of the initiating light source. On a much slower time scale, thiol-acrylates

photopolymerize in the absence of any added initiator molecules, allowing samples to be cured to depths exceeding 10 cm, and potentially improving compatibility for cell encapsulation and in situ formation in the presence of tissue. Finally, degradation behavior and network mechanical properties are controlled through changes in thiol concentration, as is the molecular weight of the degradation products.

#### Acknowledgments

The authors thank their funding sources for this work, a grant from the NIH (R01 DE12998), a Department of Education GAANN fellowship and a University of Colorado Beverly Sears Graduate Student Grant to AER. Thiol-acrylate network discussions with Sirish Reddy, as well as statistical analysis discussions with David Clough, were also very much appreciated.

#### References

- [1] Kuo CK, Ma PX. Ionically crosslinked alginate hydrogels as scaffolds for tissue engineering: Part I. Structure, gelation rate and mechanical properties. *Biomaterials* 2001;22(6):511–21.
- [2] Cao YL, Ibarra C, Vacanti C. Preparation and use of thermosensitive polymers. In: Morgan JR, Yarmush ML, editors. *Tissue Engineering: Methods and Protocols*. Totowa, NJ: Humana Press; 1999.
- [3] Kim S, Healy KE. Synthesis and characterization of injectable poly(*N*-isopropylacrylamide-*co*-acrylic acid) hydrogels with proteolytically degradable cross-links. *Biomacromolecules* 2003;4(5):1214–23.
- [4] Chen TH, Embree HD, Brown EM, Taylor MM, Payne GF. Enzyme-catalyzed gel formation of gelatin and chitosan: potential for in situ applications. *Biomaterials* 2003;24(17):2831–41.
- [5] Gutowska A, Jeong B, Jasionowski M. Injectable gels for tissue engineering. *Anat Rec* 2001;263(4):342–9.
- [6] Martens PJ, Bryant SJ, Anseth KS. Tailoring the degradation of hydrogels formed from multivinyl poly(ethylene glycol) and poly(vinyl alcohol) macromers for cartilage tissue engineering. *Biomacromolecules* 2003;4(2):283–92.
- [7] Temenoff JS, Park H, Jabbari E, Conway DE, Sheffield TL, Ambrose CG, et al. Thermally cross-linked oligo(poly(ethylene glycol) fumarate) hydrogels support osteogenic differentiation of encapsulated marrow stromal cells in vitro. *Biomacromolecules* 2004;5(1):5–10.
- [8] Behravesh E, Jo S, Zygorakis K, Mikos AG. Synthesis of in situ cross-linkable macroporous biodegradable poly(propylene fumarate-*co*-ethylene glycol) hydrogels. *Biomacromolecules* 2002;3(2):374–81.
- [9] Nguyen KT, West JL. Photopolymerizable hydrogels for tissue engineering applications. *Biomaterials* 2002;23(22):4307–14.
- [10] Burkoth AK, Anseth KS. A review of photocrosslinked polyhydrides: in situ forming degradable networks. *Biomaterials* 2000;21(23):2395–404.
- [11] Davis KA, Burdick JA, Anseth KS. Photoinitiated crosslinked degradable copolymer networks for tissue engineering applications. *Biomaterials* 2003;24(14):2485–95.
- [12] Sawhney AS, Pathak CP, Hubbell JA. Bioerodible hydrogels based on photopolymerized poly(ethylene glycol)-*co*-poly

- (alpha-hydroxy acid) diacrylate macromers. *Macromolecules* 1993;26(4):581–7.
- [13] Heller J, Fritzing BK, Ng SY, Penhale DWH. In vitro and in vivo release of levonorgestrel from poly(ortho esters) II. Cross-linked polymers. *J Controlled Rel* 1985;1:233–8.
- [14] West JL, Hubbell JA. Polymeric biomaterials with degradation sites for proteases involved in cell migration. *Macromolecules* 1999;32(1):241–4.
- [15] Lutolf MP, Raeber GP, Zisch AH, Tirelli N, Hubbell JA. Cell-responsive synthetic hydrogels. *Adv Mater* 2003;15(11):888–92.
- [16] Kurisawa M, Terano M, Yui N. Doublestimuli-responsive degradable hydrogels for drug-delivery—interpenetrating polymer networks composed of oligopeptide-terminated poly(ethylene glycol) and dextran. *Macromol Rapid Commun* 1995;16(9):663–6.
- [17] Vandijkwolthuis WNE, Franssen O, Talsma H, Vansteenbergen MJ, Vandenbosch JJK, Hennink WE. Synthesis, characterization, and polymerization of glycidyl methacrylate derivatized dextran. *Macromolecules* 1995;28(18):6317–22.
- [18] Mason MN, Metters AT, Bowman CN, Anseth KS. Predicting controlled-release behavior of degradable PLA-*b*-PEG-*b*-PLA hydrogels. *Macromolecules* 2001;34(13):4630–5.
- [19] Metters AT, Anseth KS, Bowman CN. Fundamental studies of a novel, biodegradable PEG-*b*-PLA hydrogel. *Polymer* 2000;41(11):3993–4004.
- [20] Temenoff JS, Mikos AG. Injectable biodegradable materials for orthopedic tissue engineering. *Biomaterials* 2000;21(23):2405–12.
- [21] Anseth KS, Quick DJ. Polymerizations of multifunctional anhydride monomers to form highly crosslinked degradable networks. *Macromol Rapid Commun* 2001;22(8):564–72.
- [22] Metters AT, Anseth KS, Bowman CN. A statistical kinetic model for the bulk degradation of PLA-*b*-PEG-*b*-PLA hydrogel networks. *J Phys Chem B* 2000;104(30):7043–9.
- [23] Gopferich A. Mechanisms of polymer degradation and erosion. *Biomaterials* 1996;17(2):103–14.
- [24] Temenoff JS, Athanasiou KA, LeBaron RG, Mikos AG. Effect of poly(ethylene glycol) molecular weight on tensile and swelling properties of oligo(poly(ethylene glycol) fumarate) hydrogels for cartilage tissue engineering. *J Biomed Mater Res* 2002;59(3):429–37.
- [25] Shung AK, Behravesh E, Jo S, Mikos AG. Crosslinking characteristics of and cell adhesion to an injectable poly(propylene fumarate-*co*-ethylene glycol) hydrogel using a water-soluble crosslinking system. *Tissue Eng* 2003;9(2):243–54.
- [26] Porter BD, Oldham JB, He SL, Zobitz ME, Payne RG, An KN, et al. Mechanical properties of a biodegradable bone regeneration scaffold. *J Biomech Eng—Trans ASME* 2000;122(3):286–8.
- [27] Metters AT. Investigation of degradable crosslinked hydrogels: prediction of degradation behavior (Ph.D.). Boulder, CO: University of Colorado; 2000.
- [28] Bryant SJ, Nuttelman CR, Anseth KS. Cytocompatibility of UV and visible light photoinitiating systems on cultured NIH/3T3 fibroblasts in vitro. *J Biomater Sci—Polym Ed* 2000;11(5):439–57.
- [29] Quick DJ, Anseth KS. Gene delivery in tissue engineering: a photopolymer platform to coencapsulate cells and plasmid DNA. *Pharm Res* 2003;20(11):1730–7.
- [30] Elbert DL, Hubbell JA. Conjugate addition reactions combined with free-radical cross-linking for the design of materials for tissue engineering. *Biomacromolecules* 2001;2(2):430–41.
- [31] Elbert DL, Pratt AB, Lutolf MP, Halstenberg S, Hubbell JA. Protein delivery from materials formed by self-selective conjugate addition reactions. *J Controlled Rel* 2001;76(1–2):11–25.
- [32] Lutolf MP, Hubbell JA. Synthesis and physicochemical characterization of end-linked poly(ethylene glycol)-*co*-peptide hydrogels formed by Michael-type addition. *Biomacromolecules* 2003;4(3):713–22.
- [33] Lutolf MP, Lauer-Fields JL, Schmoekel HG, Metters AT, Weber FE, Fields GB, et al. Synthetic matrix metalloproteinase-sensitive hydrogels for the conduction of tissue regeneration: engineering cell-invasion characteristics. *Proc Natl Acad Sci USA* 2003;100(9):5413–8.
- [34] Lutolf MP, Tirelli N, Cerritelli S, Cavalli L, Hubbell JA. Systematic modulation of Michael-type reactivity of thiols through the use of charged amino acids. *Bioconjugate Chem* 2001;12(6):1051–6.
- [35] Lutolf MP, Weber FE, Schmoekel HG, Schense JC, Kohler T, Muller R, et al. Repair of bone defects using synthetic mimetics of collagenous extracellular matrices. *Nat Biotechnol* 2003;21(5):513–8.
- [36] Vernon B, Tirelli N, Bachi T, Haldimann D, Hubbell JA. Waterborne, in situ crosslinked biomaterials from phase-segregated precursors. *J Biomed Mater Res Part A* 2003;64A(3):447–56.
- [37] Cramer NB, Bowman CN. Kinetics of thiol-ene and thiol-acrylate photopolymerizations with real-time Fourier transform infrared. *J Polym Sci Part A—Polym Chem* 2001;39(19):3311–9.
- [38] Posner T. Unsaturated compounds. II. Addition of mercaptans to unsaturated hydrocarbons. *Ber Deut Chem Ges* 1905;38:646–57.
- [39] Jacobine AF. In: Fouassier JD, Rabek JF, editors. Radiation curing in polymer science and technology III, polymerisation mechanisms. London: Elsevier Applied Science; 1993. p. 219.
- [40] Woods JG. Radiation curable adhesives. In: Peppas SP, editor. Radiation curing: science and technology. New York: Plenum; 1992. p. 333–98.
- [41] Metters AT, Anseth KS, Bowman CN. A statistical kinetic model for the bulk degradation of PLA-*b*-PEG-*b*-PLA hydrogel networks: incorporating network non-idealities. *J Phys Chem B* 2001;105(34):8069–76.
- [42] Berchtold KA, Bowman CN. In: RadTech Europe 99 conference proceedings, Berlin, Germany, 1999. p. 767.
- [43] Berchtold KA, Nie J, Stansbury JW, Hacıoglu B, Beckel ER, Bowman CN. Novel monovinyl methacrylic monomers containing secondary functionality for ultrarapid polymerization: steady-state evaluation. *Macromolecules* 2004;37(9):3165–79.
- [44] Cramer NB, Reddy SK, O'Brien AK, Bowman CN. Thiol-ene photopolymerization mechanism and rate limiting step changes for various vinyl functional group chemistries. *Macromolecules* 2003;36(21):7964–9.
- [45] Cramer NB, Scott JP, Bowman CN. Photopolymerizations of thiol-ene polymers without photoinitiators. *Macromolecules* 2002;35(14):5361–5.
- [46] Hoyle CE, Cole M, Bachemin M, Yoder B, Nguyen C, Kuang W, et al. In: RadTech Japan 2000 technical proceedings, 2000 December, Tokyo, Japan, 2001. p. 211.
- [47] Cramer NB, Reddy SK, Cole M, Hoyle CE, Bowman CN. Initiation and kinetics of thiol-ene photopolymerizations without photoinitiators. *J Polym Sci Part A—Polym Chem* 2004 in press.
- [48] Hoyle CE, Hensel RD, Grubb MB. Temperature-dependence of the laser-initiated polymerization of a thiol-ene system. *J Polym Sci Part A—Polym Chem* 1984;22(8):1865–73.